Chalmers Publication Library

(article starts on next page)

Plasmonic glasses: Optical properties of amorphous metal-dielectric composites

Tomasz J. Antosiewicz[1,2,*] **and S. Peter Apell**[2]

[1]*Centre of New Technologies, University of Warsaw, Żwirki i Wigury 93, 02-089 Warsaw, Poland*
[2]*Department of Applied Physics and Gothenburg Physics Centre, Chalmers University of Technology, SE-41296 Göteborg, Sweden*

[*]tomasz.antosiewicz@uw.edu.pl

Abstract: Plasmonic glasses composed of metallic inclusions in a host dielectric medium are investigated for their optical properties. Such structures characterized by short-range order can be easily fabricated using bottom-up, self-organization methods and may be utilized in a number of applications, thus, quantification of their properties is important. We show, using T-Matrix calculations of 1D, 2D, and 3D plasmonic glasses, that their plasmon resonance position oscillates as a function of the particle spacing yielding blue- and redshifts up to 0.3 eV in the visible range with respect to the single particle surface plasmon. Their properties are discussed in light of an analytical model of an average particle's polarizability that originates from a coupled dipole methodology.

OCIS codes: (240.6680) Surface plasmons; (160.4760) Optical properties; (160.4236) Nano-materials; (160.2750) Glass and other amorphous materials; (290.2200) Extinction.

References and links

1. N. Liu, M. Hentschel, T. Weiss, A. P. Alivisatos, and H. Giessen, "Three-dimensional plasmon rulers," Science **332**, 1407–1410 (2011).
2. R. Verre, K. Fleischer, J. F. McGilp, D. Fox, G. Behan, H. Zhang, and I. V. Shvets, "Controlled in situ growth of tunable plasmonic self-assembled nanoparticle arrays," Nanotechnol. **23**, 035606 (2012).
3. H. Fredriksson, Y. Alaverdyan, A. Dmitriev, C. Langhammer, D. S. Sutherland, M. Zäch, and B. Kasemo, "Hole-mask coloidal lithography," Adv. Mater. **19**, 4297–4302 (2007).
4. N. Homonnay, N. Geyer, B. Fuhrmann, and H. S. Leipner, "Advanced colloidal lithography for sub-100nm lift-off structures," Vacuum **86**, 1232–1234 (2012).
5. K. Güngör, E. Ünal, and H. V. Demir, "Nanoplasmonic surfaces enabling strong surface-normal electric field enhancement," Opt. Express **21**, 23097–23106 (2013).
6. A. A. Zakhidov, R. H. Baughman, Z. Iqbal, C. Cui, I. Khayrullin, S. O. Dantas, J. Marti, and V. G. Ralchenko, "Carbon structures with three-dimensional periodicity at optical wavelengths," Science **282**, 897–901 (1998).
7. A. Moroz, "Three-dimensional complete photonic-band-gap structures in the visible," Phys. Rev. Lett. **83**, 5274–5277 (1999).
8. W. Y. Zhang, X. Y. Lei, Z. L. Wang, D. G. Zheng, W. Y. Tam, C. T. Chan, and P. Sheng, "Robust photonic band gap from tunable scatterers," Phys. Rev. Lett. **84**, 2853–2856 (2000).
9. B. Lamprecht, G. Schider, R. T. Lechner, H. Ditlbacher, J. R. Krenn, A. Leitner, and F. R. Aussenegg, "Metal nanoparticle gratings: Influence of dipolar particle interaction on the plasmon resonance," Phys. Rev. Lett. **84**, 4721–4724 (2000).
10. C. L. Haynes, A. D. McFarland, L. Zhao, R. P. Van Duyne, G. C. Schatz, L. Gunnarsson, J. Prikulis, B. Kasemo, and M. Käll, "Nanoparticle optics: The importance of radiative dipole coupling in two-dimensional nanoparticle arrays," J. Phys. Chem. B **107**, 7337–7342 (2003).
11. B. Auguié and W. L. Barnes, "Collective resonances in gold nanoparticle arrays," Phys. Rev. Lett. **101**, 143902 (2008).

12. V. V. Gozhenko, D. A. Smith, J. L. Vedral, V. V. Kravets, and A. O. Pinchuk, "Tunable resonance absorption of light in a chain of gold nanoparticles," J. Phys. Chem. C **115**, 8911–8917 (2011).
13. T. L. Temple and D. M. Bagnall, "Optical properties of gold and aluminium nanoparticles for silicon solar cell applications," J. Appl. Phys. **109**, 084343 (2011).
14. K. Vynck, M. Burresi, F. Riboli, and D. S. Wiersma, "Photon management in two-dimensional disordered media," Nature Mater. **11**, 1017–1022 (2012).
15. M. G. Nielsen, A. Pors, O. Albrektsen, and S. I. Bozhevolnyi, "Efficient absorption of visible radiation by gap plasmon gesonators," Opt. Express **20**, 13311–13319 (2012).
16. C. Hägglund and S. P. Apell, "Plasmonic near-field absorbers for ultrathin solar cells," J. Phys Chem. Lett. **3**, 1275–1285 (2012).
17. S. Thongrattanasiri, F. H. L. Koppens, and F. J. García de Abajo, "Complete optical absorption in periodically patterned graphene," Phys. Rev. Lett. **108**, 047401 (2012).
18. C. Rockstuhl and T. Scharf, eds., *Amorphous Nanophotonics* (Springer, 2013).
19. M. Burresi, F. Pratesi, K. Vynck, M. Prasciolu, M. Tormen, and D. S. Wiersma, "Two-dimensional disorder for broadband, omnidirectional and polarization-insensitive absorption," Opt. Express **21**, A268–A275 (2013).
20. C. Helgert, C. Rockstuhl, C. Etrich, C. Menzel, E.-B. Kley, A. Tüennermann, F. Lederer, and T. Pertsch, "Effective properties of amorphous metamaterials," Phys. Rev. B **79**, 233107 (2009).
21. R. Sing, X. Lu, J. Gu, Z. Tian, and W. Zhang, "Random terahertz metamaterials," J. Opt. **12**, 015101 (2012).
22. S. Mülig, A. Cunningham, S. Scheeler, C. Pacholski, T. Bürgi, C. Rockstuhl, and F. Lederer, "Self-assembled plasmonic core-shell clusters with an isotropic magnetic dipole response in the visible range," ACS Nano **5**, 6586–6592 (2011).
23. S. N. Sheikholeslami, H. Alaeian, A. L. Koh, and J. A. Dionne, "A metafluid exhibiting strong optical magnetism," Nano Lett. **13**, 4137–4141 (2013).
24. A. V. Panov, "Impact of interparticle dipoledipole interactions on optical nonlinearity of nanocomposites," J. Mod. Opt. **60**, 915–919 (2013).
25. J. Wang and A. Z. Genack, "Transport through modes in random media," Nature **471**, 345–348 (2011).
26. D. W. Mackowski, "Calculation of total cross section of multiple-sphere clusters," J. Opt. Soc. Am. A **11**, 2851–2861 (1994).
27. E. L. Hinrichsen, J. Feder, and T. Jøssang, "Geometry of random sequential adsorption," J. Stat. Phys. **44**, 793–827 (1986).
28. T. J. Antosiewicz, S. P. Apell, M. Zäch, I. Zorić, and C. Langhammer, "Oscillatory optical response of an amorphous two-dimensional array of gold nanoparticles," Phys. Rev. Lett. **109**, 247401 (2012).
29. A. Moroz, "Depolarization field of spheroidal particles," J. Opt. Soc. Am. B **26**, 517–527 (2009).
30. B. T. Draine and P. J. Flatau, "Discrete-dipole approximation for scattering calculations," J. Opt. Soc. Am. A **11**, 1491–1499 (1994).
31. L. Zhao, K. L. Kelly, and G. C. Schatz, "The extinction spectra of silver nanoparticle arrays: Influence of array structure on plasmon resonance wavelength and width," J. Phys. Chem. B **107**, 7343–7350 (2003).
32. W. Rechberger, A. Hohenau, A. Leitner, J. Krenn, B. Lamprecht, and F. Aussenegg, "Optical properties of two interacting gold nanoparticles," Opt. Commun. **220**, 137–141 (2003).

1. Introduction

Top-down fabrication tools have enabled the study of surface plasmon resonances (SPRs) in complex nanostructures created with nanometer scale precision of shape and orientation [1]. Equally important are bottom-up methods which allow patterning long arrays [2], large surface areas with quasi-random [3] or ordered [4, 5] patterns, as well as fabricating 3D bulk synthetic opals [6]. The optical properties of such structures stem from the properties of constituent elements, however, an equally and sometimes more important contribution arises from the electromagnetic coupling within the composite. Indeed, an elegant example is the transition from a single metallic or metal-coated sphere, which exhibit a relatively simple localized SPR (LSPR), to a tunable band gap in synthetic opals assembled from such nanoparticles [7, 8]. In other structures, a shift of the SPR as a function of the array periodicity has been thoroughly investigated [9, 10]. With a proper arrangement of particles (tuning the lattice parameter) is it possible to utilize interaction between the excitation of LSPRs and diffraction to generate very narrow features in the optical spectrum in addition to the main single particle LSPR [11]. Tuning was also investigated in one-dimensional chains of ordered metallic particles in which angle dependent collective SPRs and variable absorption were observed [12].

Composite materials designed around a carefully tuned geometrical placement of constituent elements are usually susceptible to disorder which may, sometimes considerably, lower their efficiency. Because of this various studies have addressed the effects of disorder in nanocomposites [13]. Ordered systems which generate coherent optical effects, are usually characterized by either narrow-band or narrow-angle operation [14], although visible light absorption with an average efficiency of 94% using a patterned-metal/insulator/metal stack has been reported [15]. This above mentioned geometry is currently widely employed for designing perfect absorbers [16]. Indeed, particles placed over a back reflector are employed to address the problem of polarization/incident-angle dependence in perfect absorbers that operate at optical [15] or infrared [17] frequencies.

Viable routes to creating novel optical materials involve disordered or quasi-random systems [18], made using low-cost and large area bottom-up techniques. The usefulness of amorphous materials depends on how the single particle properties are modified by their quasi-random spatial distribution. Amorphous arrays of simple disks or rods retain for the most part the optical properties of the basic building block and make effective light harvesters [14, 19]. The effect of randomness has been investigated for cut-wire pair metamaterials where it was demonstrated, that the antisymmetric resonance, contrary to the symmetric one, is not affected by the degree of disorder [20]. Similarly, split ring resonators respond to disorder in a similar manner by preserving the LC and shifting the dipole resonance [21]. Magnetic activity in the visible arises in dielectric cores surrounded by disordered metal nanospheres [22, 23]. Instead of metallic inclusions, nanocomposites can have semiconducting ones in which electromagnetic interactions lead to optical nonlinearity that stems from a nonzero variance of the net dipole field in the ensemble [24]. Hence, in certain cases disorder may in fact be beneficial [25].

Here, we investigate how the optical properties of metal-dielectric ensembles change with the volume fraction of the metal inclusions. In these ensembles metal nanoparticles are arranged in a short-range ordered fashion inside a dielectric host medium (plasmonic glasses). The paper is structured as follows. We begin by discussing in Section 2 the usefulness of the T-Matrix method in these investigations and the generation scheme of amorphous arrays. Next, we present the dependence of optical spectra of plasmonic glasses on the particle density, *i.e.* the minimum center-to-center (cc) distance between the metallic inclusions. In Section 4 we derive an average particle polarizability model that matches the T-Matrix calculated spectra and use it in Section 5 to discuss the origin and evolution of the observed spectral dependence on the minimum cc distance. After the conclusions we provide appendices that give additional information on the derivation of the average polarizability of plasmonic glasses.

2. Numerical simulations – the T-Matrix method

The numerical experiments used to identify the spectral features of plasmonic glasses are conducted using the T-Matrix method [26]. Briefly, the scattered field from an arbitrary cluster of N spheres is decomposed into the sum of fields scattered by each sphere. The field acting onto the ith sphere is the sum of the incident and scattered fields of all other particles. Using the addition theorem for spherical harmonics it is possible to express those scattered fields in terms of spherical harmonics centered about sphere i. Transforming these into a cluster-centered T-matrix allows for calculation of various cross sections and other relevant quantities.

Plasmonic glass structures, shown in Fig. 1, are created using the random sequential adsorption (RSA) algorithm [27], in which spheres are sequentially added to a predefined volume (here vacuum). In each step random coordinates are chosen and if the minimum distance between the new sphere and all previously placed exceeds a minimum defined value ($r_{\text{cc}} = D\mathcal{C}$), where D is the sphere diameter and $\mathcal{C}$ is the dimensionless center-to-center distance, the new sphere joins the ensemble. This is iteratively repeated until no new sphere can be added. Here, we use a
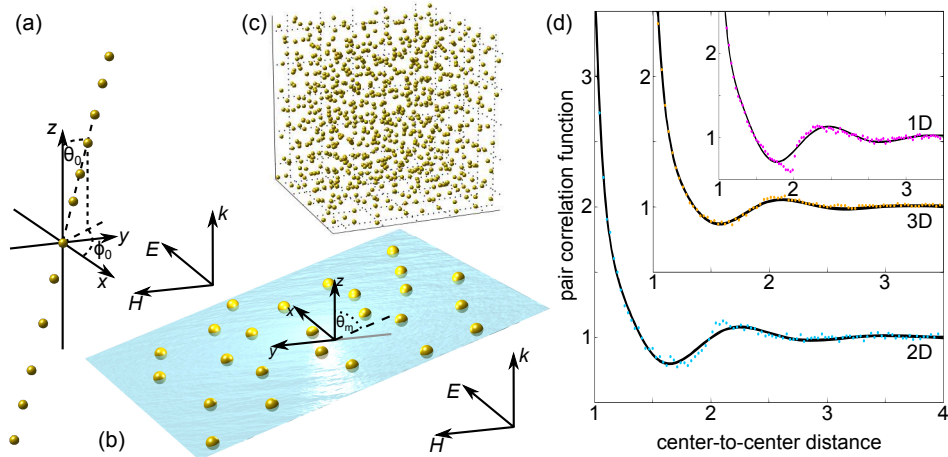
Fig. 1. Plasmonic glasses in 1-, 2-, and 3-dimensions. (a) The random chain is an array along an arbitrary direction defined by the angles θ_0 and ϕ_o. (b) The 2D amorphous array is tilted at an angle θ_m to the z-axis. (c) 3D plasmonic glass. Notice the quasi-random arrangement of particles in all displayed lattices. Spatial dimensions of the arrays are 810 μm, 9.2×9.2 μm^2, and $2 \times 2 \times 2$ μm^3, respectively for $\mathcal{C} = 1$. (d) Pair correlation functions for analyzed plasmonic glasses. The points represent data from the RSA algorithm used to generate particle position for T-Matrix calculations and the lines show the fitted functions [see Eq. (1)]. The pair correlation functions are similar; the differences in the spectra of the different glasses originate from phase space, *i.e.* the dimensionality of the system.

Drude metal ($\varepsilon(\omega) = 1 - \omega_p^2/(\omega^2 + i\gamma\omega)$, $\hbar\omega_p = 6.2$ eV, $\hbar\gamma = 0.62$ eV) spheres $D = 100$ nm in diameter. We use a count of 6000 (6k) spheres and only to assess edge effects in the 2D case we also simulate 10k particles. As it will be shown later, T-Matrix calculated resonance positions for these two cases are almost identical. To fit 6k spheres we need 810 μm, 9.2×9.2 μm^2, and $2 \times 2 \times 2$ μm^3 for 1D, 2D, and 3D, respectively for $\mathcal{C} = 1$. In the T-Matrix calculations we include the first four spherical harmonics.

Plasmonic glasses, while lacking long range order, exhibit short range correlation. This characteristic is evident in their pair correlation functions (PCFs), which are later required in the development of the analytical model. We obtain the PCF by analyzing the amorphous arrays generated by the RSA algorithm for the T-Matrix calculations and plot them in Fig. 1(d) with points. Next, we search for an analytical function $g(x)$ that fits well to the calculated data and is easily integrable when multiplied by the dipole radiation function:

$$g(x) = \Theta(x-1) \left(1 + \sin\left(\frac{x - d_1}{d_0} \right) \left(a_2 e^{-a_1(x-a_0)} + b_2 e^{-b_1(x-b_0)} \right) \right), \qquad (1)$$

where $x \equiv r/r_{cc}$ is a normalized radial parameter of the pair correlation function and $\Theta(x)$ is the Heaviside step function. Fitted PCFs for plasmonic glasses are shown in Fig. 1(d) with lines and the fitting parameters given in Table 1 in Appendix B.

3. Optical properties of plasmonic glasses

3.1. Two dimensional plasmonic glass

We begin the analysis by recalling the optical properties of a 2D plasmonic glass structure, whose oscillatory behavior in extinction has been already analyzed and compared with experimental measurements [28]. Figure 2 presents the relation between the extinction peak position
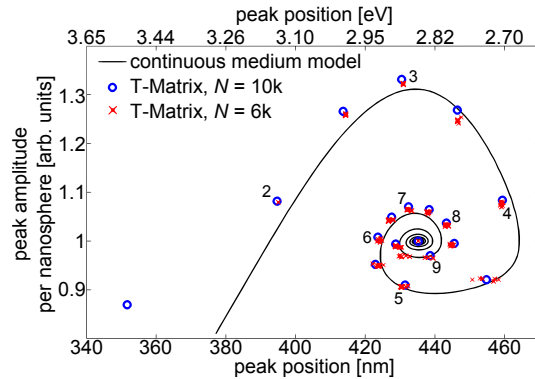
Fig. 2. Resonance amplitude per nanosphere vs. peak position for 2D plasmonic glass cal-
culated using the T-Matrix method for 6k (red crosses) and 10k spheres (blue circles). The
markers are placed every $0.5\mathcal{C}$ with numbers indicating values of $\mathcal{C}$. The continuous line
represents the peak energy calculated using an average particle polarizability approach, see
Section 4 for details. The two methods give excellent agreement down to $\mathcal{C} = 2$.

and amplitude per nanosphere. The numerical results for 10k and 6k spheres, indicated by cir-
cles and crosses, respectively, are arranged in a spiral pattern and tend to the single particle
value at 2.85 eV and normalized unity amplitude. This spiral manner of oscillations demon-
strates that the extreme values of the resonance energy and its amplitude are offset by a quarter
period. Thus, when the resonance is furthest away from the single particle value its amplitude
is approximately that of the single particle and *vice versa*. Note the small spread in numerically
obtained points for both large and small arrays, which is indicative of a relatively weak edge
effect observed for as few as 6k particles and well defined average properties of these glasses.
The only exception is observed for $\mathcal{C} = 4.5$. The reason for this is the close matching of the
resonance position (*ca.* 450 nm) to the minimum distance between the particles (also 450 nm),
resulting in in-phase coupling of neighboring spheres. For this cc value small changes in posi-
tioning may lead to comparatively large changes in the spectral response at resonance. Finally,
we point out that the line marking the analytically calculated resonance position (see derivation
of the model in Sec. 4), follows closely the T-Matrix results.

In the next section we will now show optical results for 1D plasmonic glass (an amorphous
chain) under various directions of illumination. This is important, as in a qualitative picture,
materials with higher dimensionality (2D, 3D) may be derived from appropriate assembling of
a number of 1D chains. Thus, as will be shown subsequently, their properties stem from those
of amorphous chains.

3.2. One dimensional plasmonic glass

We begin the plasmonic chain results by showing the optical cross sections of a normally il-
luminated amorphous chain of metal spheres in Fig. 3(a) and 3(b). The electric field can be
aligned either perpendicular to or along the chain, see Fig. 3(a) and 3(b), respectively. Markers
show T-Matrix results, while the three thin horizontal lines indicate the single particle reso-
nance positions of scattering, extinction, and absorption. The oscillatory behavior of the optical
response is immediately visible, however, the oscillations are considerably more pronounced
for the electric field perpendicular to the chain as the peak position varies over 0.4 eV, while for
parallel orientation only over 0.15 eV. Again, the blue lines mark the results of the analytical
model detailed in the next section.

Figure 3(c) shows the dependence of the plasmon peak position of an amorphous chain of
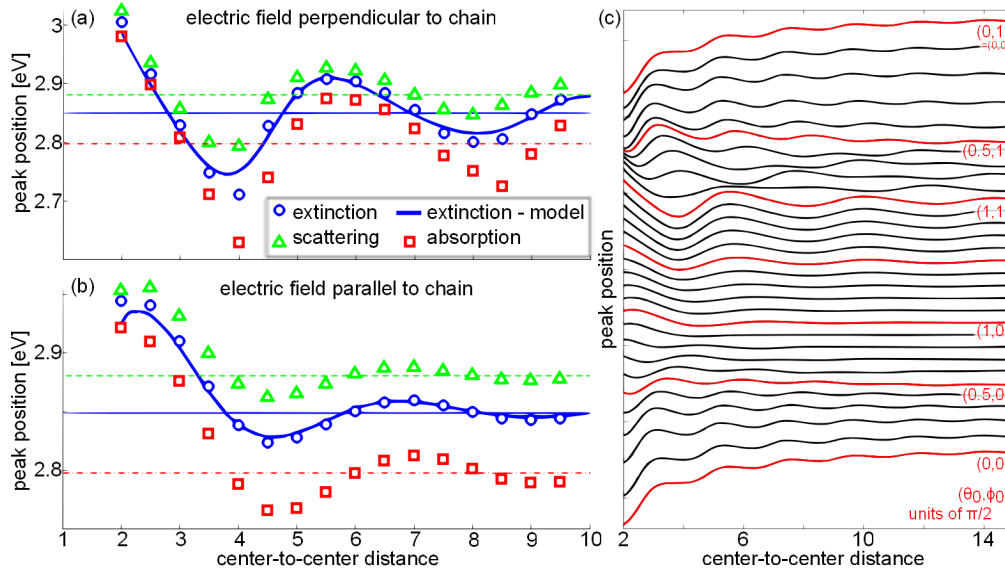
Fig. 3. Optical cross sections of an amorphous chain of particles normally illuminated with (a) the electric field perpendicular and (b) parallel to the chain. Resonance positions are calculated using the T-Matrix method (markers) and the analytically calculated average medium extinction (thick line). The thin horizontal lines mark respective single particle values. (c) Extinction peak position evolution with changing orientation relative to the incident wave. The chain orientation starts from (0,0) – wave incident along the chain, tilts to (1,0) – electric field parallel to the chain, rotates to (1,1) – electric field perpendicular to chain, and tilts back to (0,1). The angles are in units of $\pi/2$ for (θ_0, ϕ_0). Notice the very strong redshift of the plasmon peak for a chain illuminated along its length. As the incidence angle is decreased the redshift diminishes and only very small oscillations remain. Rotating the chain from parallel to perpendicular relative to the electric field amplifies the oscillations to maximum amplitude. The final tilting back to the grazing incidence restores the strong redshift.

spheres as a function of the minimum cc distance between spheres and the direction of the chain relative to the incident wave. The angles, expressed in units of $\pi/2$, vary from $(\theta_0 = 0, \phi_0 = 0)$ – incidence along the chain – to normal incidence for the electric field parallel to the chain (1,0) and perpendicular to it (1,1). When light propagates along the chain the optical response is shifted by 0.5 eV to the red from the single particle resonance. Additionally, small oscillations are superimposed onto the redshift. As the chain is tilted in θ to (0.5,0) the redshift decreases quickly, followed by an almost complete disappearance of the oscillations at (1,0) with the exception for small cc values (less than 0.1 eV difference relative to the single particle value). As the chain is rotated towards perpendicular orientation relative to the electric field the oscillations increase to their maximum value of 0.15 eV. The subsequent tilting in θ to grazing incidence restores the slightly modulated redshift.

3.3. Three dimensional plasmonic glass

The optical properties of 3D plasmonic glass are shown in Fig. 4, with markers representing T-Matrix simulation results. The most apparent feature, especially when compared to previously described lower dimensional structures, is a lack of large oscillations of the peak positions. All optical cross section resonances exhibit a steady redshift with scattering showing the strongest
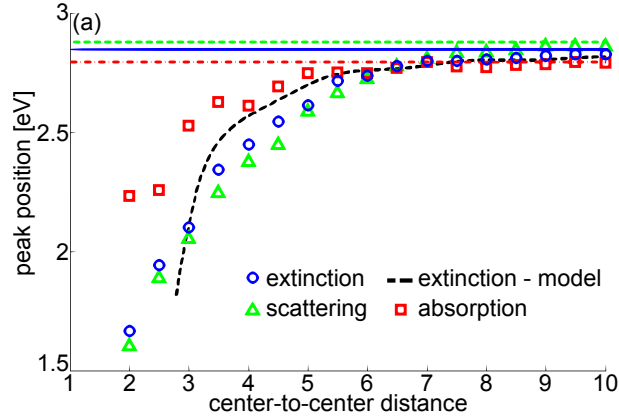
Fig. 4. Peak positions of extinction, absorption, and scattering cross sections of 3D plasmonic glass with 6k spheres calculated using the T-Matrix method. Markers show cc dependence, while horizontal lines indicate single particle values. The black dashed line shows the analytically obtained extinction peak position which agrees very well down to $\mathcal{C} = 5$, between 3 and 5 it underestimates the peak shift, while below 3 overestimates it. However, a consistent redshift of all cross sections is demonstrated.

redshift down to a value of 1.6 eV at $\mathcal{C} = 2$ from a single particle value of 2.9 eV. The absorption peak shift is much smaller and it can be seen that the relation of the absorption and scattering peaks is exchanged. For sparse arrays (and indeed for the single particle) scattering is to the blue of the absorption peak, but for $\mathcal{C} \approx 6$ this reverses. The analytical description of the average properties is less accurate than in the low dimensional materials with the extinction cross section being accurate only down to a cc distance of $\mathcal{C} = 5$. For denser glasses the peak shift is only qualitatively accurate showing a larger red shift for $\mathcal{C} = 2$ than obtained from the T-Matrix formalism.

4. Continuous-dipolar-medium approach

The T-Matrix method is a powerful tool to calculate scattering from the plasmonic glasses, however, it is somewhat limited in explaining the processes occurring within them. Taking into account as a first approximation only dipolar interactions, we assume that the bulk optical response of plasmonic glasses stems from the single particle polarizability α and is further modified by interparticle coupling. The polarizability of a spherical nanoparticle in the modified long wavelength approximation (MLWA) [29] is $1/\alpha = 1/\alpha^q - (\frac{2}{3}ik^3 + \frac{k^2}{s})/(4\pi\varepsilon_0)$, where $\alpha^q = 4\pi\varepsilon_0 R^3(\varepsilon - 1)/(\varepsilon + 2)$ is the quasistatic polarizability, for simplicity, in vacuum, $k = 2\pi/\lambda$, ε is the permittivity of the particle, and s is a length associated with the particle size.

For a given sphere arrangement it is natural to describe the dipole-dipole interactions using the coupled dipole approximation (CDA) [30]. The local field acting onto particle i, including the contribution from all other particles (j), is $\mathbf{E}_{\text{loc},i} = \mathbf{E}_{\text{inc},i} - \sum_{j \neq i} \mathbf{A}_{ij} \mathbf{P}_j$, where we assume that the incident field propagates along the z-axis $\mathbf{E}_{\text{inc}} = \mathbf{E}_0 e^{ikz}$ and $\mathbf{A}_{ij}\mathbf{P}_j$ determines the dipole radiation. It is important to notice, that in a medium composed of identical average particles the polarizability of each is the same, albeit shifted in phase with respect to each other. Here we define the average particle as having the same optical spectrum as the ensemble except for the amplitude which is N times smaller. Setting as a point of reference a particle placed in the center of the coordinate system (having $\mathbf{P}_0$), the polarization of all other average particle j located in a plane with coordinate z_j is $\mathbf{P}_j = \mathbf{P}_0 e^{ikz_j}$.

The self-consistently calculated polarizability of an average particle $\boldsymbol{\alpha}^*$ is thus

$$(\boldsymbol{\alpha}^*)^{-1} = (\boldsymbol{\alpha})^{-1} + \mathcal{S}, \tag{2}$$

where $\boldsymbol{\alpha}$ is the polarizability tensor of a single nanoparticle and we introduce a coupling term $\mathcal{S} \equiv \sum_{j \neq 0} \mathbf{A}_{0j} e^{ikz_j}$ which runs over all other particles [31]. The summation value is defined by the spatial arrangement of matter in the structure which can take any arbitrary form. Here, we recast $\mathcal{S}$ as an integral of a structure factor over the volume occupied by the object (see Appendix A for details). For the structures considered here the structure factor is the PCF $g(r)$ which describes the stochastic arrangement of particles. Dropping the tensor formalism and assuming linearly polarized light in the x direction, the interaction term becomes

$$\mathcal{S} = \sigma \int e^{ikz} A_{xx} g(r) \, \mathrm{d}V, \tag{3}$$

where $\sigma = \sigma_0 / r^d$ is the particle density in the considered dimensionality ($d = 1, 2, 3$ for 1D, 2D, and 3D, respectively), σ_0 is a packing parameter, and A_{xx} is given by Eq. (12) in Appendix A. Thus, the polarizability of the medium becomes

$$\alpha^* = \frac{1}{\alpha^{-1} + \mathcal{S}}. \tag{4}$$

Using Eq. (4), extinction is calculated as $C_{\mathrm{ext}} \propto k \mathrm{Im}(\alpha^*)$. From these calculations we extract the resonance positions for all considered plasmonic glasses and plot them in preceding figures together with the T-Matrix results. The key to calculating the average particle properties lies in evaluating Eq. (3) to yield $\mathcal{S}$ for all dimensionalities, which are given in Appendix B.

5. Discussion

For a qualitative analysis, let us first recall the optical properties of two identical metal particles side-by-side [32]. An electric field parallel to the long axis of the dimer induces an attractive configuration of dipoles in the particles leading to a lower resonance energy. When the field is aligned along the short axis, a repulsive dipolar arrangement results in a higher energy mode. In the 1D case, see Fig. 3(c), there are three distinct arrangements: (1,0), (1,1), and (0,0) in terms of the orientation of the particle chain. In the first case the electric field is aligned along the chain while in the other two across. This means, that for the (1,0)-orientation the particles are predominantly coupled by their near-fields and oscillations are weak, while retardation inherent to dipolar radiation determines the color of the oscillation. Strong coupling will only be observed for dense placement and results in a strong redshift for $\mathcal{C} < 2$, as reported by Rechberger *et al.* [32].

The remaining two field-chain orientations are similar in this respect that the induced dipoles are perpendicular to the chain meaning that both near- and far-field interactions take place. Due to involvement of far-fields, oscillations are present up to much larger cc values than for the (1,0)-orientation. The major difference responsible for their different optical properties is the constant phase of the particle polarization for the (1,1)-orientation and a linearly varying for (0,0). In the (1,1) case particles placed on opposite sides of the central one will illuminate it in-phase. Depending on the sign of the radiated field with respect to the incident one the oscillations will induce either a blue- or redshift. And in contrast to the (1,0) case, due to the repulsive alignment of the induced dipoles, for dense packing for the (1,1)-orientation experiences a blue shift for small cc values.

In an amorphous chain illuminated along its length the phase of the induced dipoles depends linearly on their z-position. This means, that two hypothetical particles placed symmetrically

to either side of the central one have a phase shift of $e^{\pm ikz}$ relative to the central one. Adding the retardation phase shift as well as a small Δ phase delay due to reradiation, the scattered fields of the preceding one will illuminate the central one with a phase shift of $e^{i\Delta}$, while the following one with $e^{2ikz+i\Delta}$. This means, that the coupling will be attractive for certain values of the minimum cc distance resulting in a redshift, as seen for the (0,0)-orientation. However, if we considered unphysical values of the cc distance smaller than one (mathematically overlapping particles with no common volume), then the phase shifts due to particle positioning would be very small and repulsive interaction would be restored giving an expected blue shift [32]. Of course, this does not include higher order multipoles that are present for $\mathcal{C} < 2$ and will influence the optical response, however, we do not consider them in the analytical model.

The influence of interparticle coupling in 1D glass is also apparent in absorption and scattering, however, the modulation depths of absorption and scattering are not equal. Figure 3(a) illustrates this fact clearly: scattering is less affected by radiation from other particles in comparison to absorption. The oscillation amplitudes at $\mathcal{C} = 4$ are 0.09 eV and 0.17 eV for scattering and absorption, respectively. Noting that extinction is a sum of the other two cross sections, we have the extinction cross section expressed as

$$C_{\text{ext}} \propto \text{Im} \frac{\alpha}{1 + \alpha \mathcal{S}} = \frac{\text{Im}(\alpha) - |\alpha|^2 \text{Im}(\mathcal{S})}{|1 + \alpha \mathcal{S}|^2}, \tag{5}$$

and the scattering cross section is

$$C_{\text{sca}} \propto \frac{|\alpha|^2}{|1 + \alpha \mathcal{S}|^2}. \tag{6}$$

For individual particles α is constant, but the coupling term $\mathcal{S}$ varies as the minimum cc distance changes. In the case of scattering, only the denominator is a function of the coupling term, but for extinction also the numerator is a function of $\mathcal{S}$, thus the oscillations of extinction are indeed larger than for scattering. Furthermore, with extinction being the sum of scattering and absorption, it is reasonable that absorption experiences larger oscillations than scattering.

One way of looking at the 2D and 3D glasses is that they may be constructed from amorphous chains. While this is a slight simplification, as structures constructed this way would display some degree of order, it helps to qualitatively consider the emergence of the observed 2D and 3D glass properties. In the 2D case for normal illumination the strong oscillations and blueshift at small cc values ($\mathcal{C} \sim 2$) is expected, as it can be viewed as a combination of the 1D (1,0)- and (1,1)-orientations (in-phase excitation), which both exhibit a blueshift and the latter one strong oscillations.

For 3D plasmonic glass the central particle is surrounded by a virtual shell of small polarized dipoles. The phase difference between the *front* and *back* halves induces a redshift for all dipole orientations, similar as in the 1D (0,0) chain orientation, and this coupling is always strong, as it occurs via both near- and far-field coupling. On the other hand, the interaction between the central particle and the *left/right* sides depends on their relative phases and the resulting blueshift (at small cc values) is weaker than the redshift. Thus, 3D glass exhibits a redshift of the resonance position for decreasing $\mathcal{C}$.

Finally, we comment on the accuracy of the analytical treatment with respect to the exact T-Matrix solution. For 1D structures the agreement is excellent in the whole considered cc range and for 2D only marginally worse. The accuracy decreases for 3D glasses and in part of the cc range only qualitative agreement is noted. The two possibilities for this are a relatively larger contribution from edge effects than in lower dimensionalities and a possible increase of the importance of the quadrupole mode. Remaining is an almost complete disappearance of oscillations in the 3D case. To observe oscillations a clear geometry for inducing oscillations

is required. In the 1D case the strongest oscillations are observed for normal incidence [in Fig. 3(c) – (1,1)], where the effective dipole medium on both sides of the average particle is in phase. When illuminated along the chain the dipole medium is not in phase and oscillations are weaker. For a 3D situation the phase can not be matched and oscillations disappear.

6. Conclusions and summary

Plasmonic glasses, composite materials which are characterized by an amorphous distribution of metallic inclusions in a host matrix in the form of chains, planar arrays or 3D structures, exhibit a number of interesting optical properties. The single particle polarizability (resonance of a single inclusion) is considerably modified via coupling to other inclusions. Using T-Matrix calculations for amorphous arrays of up to 10k spheres and for a wide range of inclusion densities, *i.e.* minimum cc values, we have demonstrated significant changes to the optical cross sections.

Depending on the dimensionality of the plasmonic glass, polarization, and direction of illumination the optical response may: (i) exhibit significant oscillations of 0.2 eV or more (normal incidence for 1D and 2D glasses), or (ii) show a very significant redshift of up to 0.4 eV with small or negligible oscillations (grazing incidence for 1D or 3D glasses). Furthermore, using a continuous dipolar medium approach based on the CDA we have analytically derived the average polarizability of the glasses that is in agreement with the T-Matrix calculations and elucidates the origin of observed spectral changes. These results show how the optical properties of amorphous 1D, 2D, and 3D plasmonic arrays depend on the particle density, especially for small interparticle spacing. These dependencies need to be taken into account when designing functional amorphous bottom-up fabricated materials. The importance of our finding depends on the particular application. For example, in 2D ensemble LSPR sensors the shift might not be important as long as the sensitivity per refractive index unit is good, however, validation of peak position and shape might only be adequate (qualitative). On the other hand, when attempting to position the LSPR to the blue of the bandgap of a semiconductor for plasmon enhanced photovoltaics a shift of the resonance position of 20–40 nm might cause a significant decrease of the efficiency. A similar problem occurs when trying to couple LSPRs to molecular resonances. Our results are applicable not only to simple inclusions, but also to materials with complex ones [22, 23] and can be extended to include interaction of higher order modes.

Appendix A: Continuous-dipolar-medium approach

Here we expand the theoretical derivation of Eqs. (3) and (4) from the CDA equations for greater clarity. The starting point is an equation for the local fields acting onto particles in the amorphous arrays. The field acting onto particle i including the contribution from all other particles (j) in the CDA is $\mathbf{E}_{\mathrm{loc},i} = \mathbf{E}_{\mathrm{inc},i} - \sum_{j \neq i} \mathbf{A}_{ij} \mathbf{P}_j$, where we assume that the incident field propagates along the z-axis $\mathbf{E}_{\mathrm{inc}} = \mathbf{E}_0 e^{ikz}$ and $\mathbf{A}_{ij} \mathbf{P}_j$ determines the dipole radiation. The important assumption here is that the polarizability of average particles in a medium composed of such particles is the same. However, a defined axis of light propagation (z-axis) causes a phase shift of e^{ikz}. This means, that the polarization of an average particle j located in a plane with coordinate z_j is

$$\mathbf{P}_j = \mathbf{P}_0 e^{ikz_j}, \tag{7}$$

where $\mathbf{P}_0$ is the polarization of the particle in the center of the coordinate system. Thus, the field polarizing the average sphere at the center of the coordinate system ($i = 0$) and the resulting average polarizability $\boldsymbol{\alpha}^*$ can now be written as

$$\mathbf{E}_{\mathrm{loc},0} = \mathbf{E}_0 - \sum_{j \neq 0} \mathbf{A}_{0j} \mathbf{P}_j = \mathbf{E}_0 - \mathbf{P}_0 \sum_{j \neq 0} \mathbf{A}_{0j} e^{ikz_j}. \tag{8}$$

The polarization of the average particle is $\mathbf{P}_0 = \boldsymbol{\alpha}\mathbf{E}_{\text{loc},0}$ and after substituting into it Eq. (8) we get

$$\mathbf{P}_0\left(1 - \boldsymbol{\alpha}\sum_{j\neq 0}\mathbf{A}_{0j}e^{ikz_j}\right) = \boldsymbol{\alpha}E_{\text{loc},0} \quad \Rightarrow \quad \boldsymbol{\alpha}^* = \frac{\mathbf{P}_0}{\mathbf{E}_{\text{loc},0}} = \frac{\boldsymbol{\alpha}}{1 - \boldsymbol{\alpha}\sum_j \mathbf{A}_{0j}e^{ikz_j}}, \tag{9}$$

where $\boldsymbol{\alpha}$ is the polarizability tensor of a single nanoparticle. In the above equation the single particle polarizability $\boldsymbol{\alpha}$ is modified by a term arising from the coupling $\mathcal{S} \equiv \sum_{j\neq 0}\mathbf{A}_{0j}e^{ikz_j}$. This term can be rewritten in the following form

$$\sum_{j\neq 0}\mathbf{A}_{0j}e^{ikz_j} = \sum_{j\neq 0}\int \delta(\mathbf{x}-\mathbf{x}_j)\mathbf{A}_{0j}e^{ikz_j}\,dV, \tag{10}$$

where $\delta(\mathbf{x}-\mathbf{x}_j)$ describes the particle arrangement in space. We change the order of the integral and the sum and let $G(\mathbf{x}) \equiv \sum_{j\neq 0}\delta(\mathbf{x}-\mathbf{x}_j)$ be a structure factor. Thus, the interaction term now depends on the function $G(\mathbf{x})$ which can describe any particle arrangement. In the considered case of a plasmonic glass, the distribution of metal particles is quasi-random with distinct short-range order and lack of long-range order. The stochastic nature of this arrangement is best described by a PCF, see Fig. 1(d). In order to assure the correct dimensionality of the integral the PCF is multiplied by the average particle density σ. We let $G(\mathbf{x}) \equiv \sigma g(r)$, where $g(r)$ is the PCF. Thus dropping the tensor formalism and assuming linearly polarized light in the x direction, the interaction term becomes

$$\mathcal{S} = \sigma\int e^{ikz}A_{xx}g(r)\,dV, \tag{11}$$

where A_{xx} in usual spherical coordinates (r,θ,ϕ) is

$$A_{xx} = \frac{1}{4\pi\varepsilon_0}e^{ikr}\left[\frac{k^2}{r}\left(-\sin^2\theta\sin^2\phi - \cos^2\theta\right) + \frac{1-ikr}{r^3}\left(1 - 3\sin^2\theta\cos^2\phi\right)\right]. \tag{12}$$

Consideration of only the A_{xx} term in the analytical treatment is justified by the fact that in calculating the off-diagonal terms one needs to perform an azimuthal integral which yields zero. They are $A_{xy} \propto \int_0^{2\pi}\sin\phi\cos\phi\,d\phi$ and $A_{xz} \propto \int_0^{2\pi}\cos\phi\,d\phi$. This is a consequence of the averaging inherent to our approach, however, in a real glass y- and z-components of polarization will be present due to the randomness in particle arrangement.

Appendix B: Analytical description of plasmonic glasses

Three dimensional plasmonic glass. The largest structure is a 3D amorphous array, Fig. 1(c), yet it is the simplest to analyze due to its symmetry – the equations do not depend on the

Table 1. Fitting parameters for pair correlation functions [see Eq. (1)] of plasmonic glasses in 1-, 2-, and 3-dimensions shown in Fig. 1.

dimension	parameter							
	a	a_0	a_1	b	b_0	b_1	d	e
1D	22.	0.87	15.	0.22	2.1	1.19	0.79	1.39
2D	1.02	1.05	17.5	0.77	0.87	1.62	0.79	1.22
3D	1.47	1.03	15.	0.64	0.71	1.74	0.81	1.08

direction of incidence and polarization. The 3D interaction term is

$$\mathcal{S}^{3D} = \sigma \int\limits_{r_{cc}}^{+\infty} \int\limits_{0}^{\pi} \int\limits_{0}^{2\pi} r^2 \sin\theta\, e^{ikr\cos\theta} A_{xx} g(x)\, \mathrm{d}r\, \mathrm{d}\theta\, \mathrm{d}\phi. \tag{13}$$

Parts of the integrations to be performed here will diverge, unless a cutoff is introduced. To this end we use the function e^{-ar}, which can physically be understood as an illuminating beam of a finite cross section, where a determines how quickly the beam amplitude decays.

Two dimensional plasmonic glass. Here, we give the 2D interaction term for an amorphous array illuminated by an arbitrarily incident s-polarized (TE) light, while for p-polarized (TM) the electric field is rotated by $\frac{\pi}{2}$. The difference between this and the 3D case is the restriction of the integral to a plane. The plane is tilted in the yz-plane and is given by $z = By$ [see Fig. 1(b)], where the slope is $B = \cot\theta_m$ and θ_m is the angle between the z-axis and the 2D plane. For TE light we have in spherical coordinates $\theta = \mathrm{arccot}(\cot\theta_m \sin\phi)$ which indicates, that for every angle ϕ there is a certain angle θ which defines a part of the 2D plane. Thus the integral is multiplied by $\frac{1}{r}\delta(\theta - \mathrm{arccot}(\cot\theta_m \sin\phi))$ to define the array plane

$$\mathcal{S}^{2D} = \sigma \int\limits_{r_{cc}}^{+\infty} \int\limits_{0}^{\pi} \int\limits_{0}^{2\pi} r \sin\theta\, e^{ikr\cos\theta} A_{xx} \delta[\theta - \mathrm{arccot}(\cot\theta_m \sin\phi)] g(x)\, \mathrm{d}r\, \mathrm{d}\theta\, \mathrm{d}\phi. \tag{14}$$

For normally incident light the delta function is nonzero only for $\theta = \pi/2$ and Eq. (14) simplifies to the case described previously [28].

Random chain – 1D plasmonic glass. An amorphous linear chain of particles, due to its linearity, can be arbitrarily oriented in 4π relative to the incident wave. Figure 1(a) shows the geometry where the chain orientation is defined by a polar angle θ_0 and an azimuthal ϕ_0. To confine the integration volume to the chain we write the integral in two parts $\delta(\theta - \theta_0)\delta(\phi - \phi_0)$ and $\delta(\theta - (\pi - \theta_0))\delta(\phi - (\phi_0 + \pi))$ with both expressions divided by $r^2 \sin\theta$. This simplifies the integrations to only the radial one

$$\mathcal{S}^{1D} = \sigma \int\limits_{r_{cc}}^{+\infty} (e^{ikr\cos\theta_0} + e^{-ikr\cos\theta_0}) A_{xx} g(x)\, \mathrm{d}r. \tag{15}$$

Acknowledgments